Journal of Solid State Chemistry 182 (2009) 709–715

Contents lists available at ScienceDirect

Journal of Solid State Chemistry

journal homepage: www.elsevier.com/locate/jssc

Crystal structures and magnetic properties of fluorite-related oxides Ln_3NbO_7 (Ln = lanthanides)

Yoshihiro Doi *, Yuka Harada, Yukio Hinatsu

Division of Chemistry, Graduate School of Science, Hokkaido University, Sapporo 060-0810, Japan

ARTICLE INFO

Article history:
Received 22 July 2008
Received in revised form
10 October 2008
Accepted 9 December 2008
Available online 31 December 2008

Keywords:
Fluorite-related oxide
Lanthanide
Magnetic susceptibility
Specific heat
Antiferromagnetic transition

ABSTRACT

Crystal structures and magnetic properties of the ternary oxides Ln_3NbO_7 (Ln = La, Pr, Nd, Sm–Lu) are reported. Their powder X-ray diffraction measurements and Rietveld analyzes show that they have the fluorite-related structures with space group *Pnma* (Ln = La, Pr, Nd), $C222_1$ (Ln = Sm–Tb), or *Fm*-3*m* (Ln = Dy–Lu). Magnetic susceptibility measurements were carried out from 1.8 to 400 K. The Ln_3NbO_7 compounds for Ln = Pr, Gd, Dy–Yb show Curie–Weiss paramagnetic behavior, and Sm_3NbO_7 and Eu_3NbO_7 show van Vleck paramagnetism. On the other hand, two magnetic anomalies were observed for both Nd_3NbO_7 (0.6 and 2.7 K) and Tb_3NbO_7 (2.0 and 3.2 K). From the results of specific heat measurements, it was found that these anomalies are due to the antiferromagnetic ordering of Ln ions in two different crystallographic sites (the 8-coordinated and 7-coordinated sites).

1. Introduction

Compounds containing lanthanide (Ln) ions have been attracting interest since they often show anomalous magnetic properties derived from the unpaired 4*f* electrons at low temperatures. Among them, much attention has been paid to the ternary oxides Ln_3NbO_7 [1–9]. The niobium ion in these compounds adopts the pentavalent state and is diamagnetic; thus, the magnetic properties of Ln_3NbO_7 are due to the behavior of Ln^{3+} ions. The structure of Ln_3NbO_7 compounds show polymorphic modifications based on a fluorite-type lattice: some cation-ordered structures for larger Ln ions (Ln = La–Nd, Sm–Tb) [1–9] and a cation-disordered structure for smaller ones (Ln = Y, Dy–Lu) [2,6,9]. In spite of many structural studies on Ln_3NbO_7, structural parameters were not determined for more than half of these compounds, and some different models were suggested for one compound.

Recently, electrical and magnetic of related Ln_3MO_7 compounds (M = Mo [10,11], Ru [12–19], Ir [20–22], Os [19,23,24], and Re [25–27]) were widely investigated from viewpoint of their one-dimensional nature. In these cases, both the paramagnetic Ln^{3+} and M^{5+} ions contribute to the magnetic properties of Ln_3MO_7 compounds, and their magnetic behavior is complicated. On the other hand, it was found that Ln_3MO_7 compounds with the diamagnetic Ta^{5+}, Nd_3TaO_7 and Tb_3TaO_7, bring about an interesting "two-step" antiferromagnetic transition due to the ordering of Ln magnetic moments in different crystallographic sites [28]. As for Ln_3NbO_7 compounds, low-temperature magnetic properties were unknown except for Ln = Gd, Dy and Ho. The Ho_3NbO_7 shows an antiferromagnetic transition at ~1 K, and Gd_3NbO_7 and Dy_3NbO_7 are paramagnetic down to 1 K [29].

In order to obtain systematic information about crystal structures and elucidate the detailed magnetic properties for Ln_3NbO_7, we have performed powder X-ray diffraction (XRD), magnetic susceptibility and specific heat measurements. These results will be discussed here.

2. Experimental

2.1. Sample preparation

Polycrystalline samples Ln_3NbO_7 were prepared by the solid-state reaction. As starting materials, Ln_2O_3 (Ln = La, Nd, Sm–Gd, Dy–Lu), Pr_6O_{11}, Tb_4O_7 (Nippon Yttrium, 99.9%), and Nb metal (Kojundo Chem. Lab., 99.9%, powder) were used. Before use, La_2O_3 and Nd_2O_3 were dried at 1173 K overnight. These reagents were weighed in appropriate metal ratios and ground intimately in an agate mortar. The mixtures were pressed into pellets and then heated in air at 1773 K for 24–36 h with intermediate regrinding and repelletizing until a single phase was obtained. For only Pr_3NbO_7, 10 mol% excess Pr_6O_{11} was used to prevent a formation of an impurity phase $PrNbO_4$ [30]. After heating at 1773 K for 36 h, the residual praseodymium oxide was dissolved by the diluted nitric acid (0.1 M).

* Corresponding author. Fax: +81 11 706 4931.
E-mail address: doi@sci.hokudai.ac.jp (Y. Doi).

0022-4596/$ - see front matter © 2008 Elsevier Inc. All rights reserved.
doi:10.1016/j.jssc.2008.12.012

2.2. Powder XRD measurements

The powder XRD measurements were performed at room temperature in the range $10^\circ \leqslant 2\theta \leqslant 120^\circ$ using a 2θ step size of 0.02° with CuKα radiation on a Rigaku MultiFlex diffractometer. The XRD data were analyzed by the Rietveld technique, using the program RIETAN2000 [31].

2.3. Magnetic susceptibility and specific heat measurements

The temperature dependence of the magnetic susceptibility was measured under both zero-field-cooled (ZFC) and field-cooled (FC) conditions in an applied field of 0.1 T over the temperature-range 1.8–400 K using a SQUID magnetometer (Quantum Design, MPMS-5S). The samples were contained in diamagnetic capsules, and the data were corrected by extracting the contribution from diamagnetic ionic susceptibilities. For La_3NbO_7, Nd_3NbO_7 and Tb_3NbO_7, specific heat measurements were performed using a relaxation technique with a commercial physical property measurement system (Quantum Design, PPMS model) in the temperature range 0.5–25 K (or 1.8–300 K). The sintered sample in the form of a pellet was mounted on a thin alumina plate with Apiezon N grease for better thermal contact. Heat capacity of the sample was obtained by subtracting the addenda heat capacity, which had been determined in a separate run without the sample.

3. Results and discussion

3.1. Crystal structures of Ln_3NbO_7

The Ln_3NbO_7 compounds with Ln = La, Pr, Nd, Sm–Lu were successfully prepared. The XRD patterns for the La, Eu, and Lu compounds are shown in Fig. 1. The results indicate that these compounds adopt three kinds of crystal structures reflecting the changing size of the Ln^{3+} ion.

For compounds with larger Ln ions (Ln = La, Pr, Nd), the XRD patterns were indexed with an orthorhombic unit cell. According to earlier works [3–5,7], at least two models for orthorhombic structures have been proposed: the space group *Cmcm* with $a \sim 2a_f$, $b \sim \sqrt{2}a_f$, $c \sim \sqrt{2}a_f$ [4,7] and *Pnma* with $a \sim \sqrt{2}a_f$, $b \sim 2a_f$, $c \sim \sqrt{2}a_f$ [3,5] (a_f: the unit cell of the fluorite structure). We analyzed the present data by the Rietveld method using some structural models including these described above. The inset graph of Fig. 1(a) shows a comparison of the Bragg reflections between the *Cmcm* and *Pnma* models. If we assume the *Cmcm* model, some reflection peaks cannot be explained from the extinction condition (e.g., the peak at $2\theta \sim 16.5^\circ$ corresponding to the 011 reflection). In the case of the *Pnma* model, the calculated and observed profiles give a very good agreement (see Fig. 1(a)); thus, we finally adopted this model for the structural analyzes.

The XRD profiles (Fig. 1(b)) for the Ln_3NbO_7 with intermediate sized Ln ions (Ln = Sm–Tb) can be indexed also by an orthorhombic unit cell. However, some reflections (e.g., the peak at $2\theta \sim 20.4^\circ$ corresponding to the 201 reflection) that are absent in both *Pnma* and *Cmcm* are observed. This fact indicates that these structures have a different symmetry. The space group $C222_1$ (the cell dimension $a \sim 2a_f$, $b \sim \sqrt{2}a_f$, $c \sim \sqrt{2}a_f$) proposed for Gd_3NbO_7 [4] fulfills this reflection condition; thus, we analyzed the data using this model.

The Ln_3NbO_7 with smaller Ln ions (Ln = Dy–Lu) show simple XRD patterns (Fig. 1(c)) indexed with a cubic cell of the fluorite-type structure [6,9]. In this structure, the Ln and Nb ions randomly occupy the cation site (4*a* site in the space group *Fm*-3*m*) in the ratio of 3:1, and 1/8 of the oxide ions are randomly defective at the anion site (8*b* site); more properly, their formula unit can be represented as $Ln_{0.75}Nb_{0.25}O_{1.75}$. The calculated profiles for Ln_3NbO_7 (Ln = Nd, Eu and Lu) are plotted in Fig. 1, and the refined structural parameters are listed in Tables 1–3, respectively. The structural parameters for the other compounds are shown in Supplementary Tables.

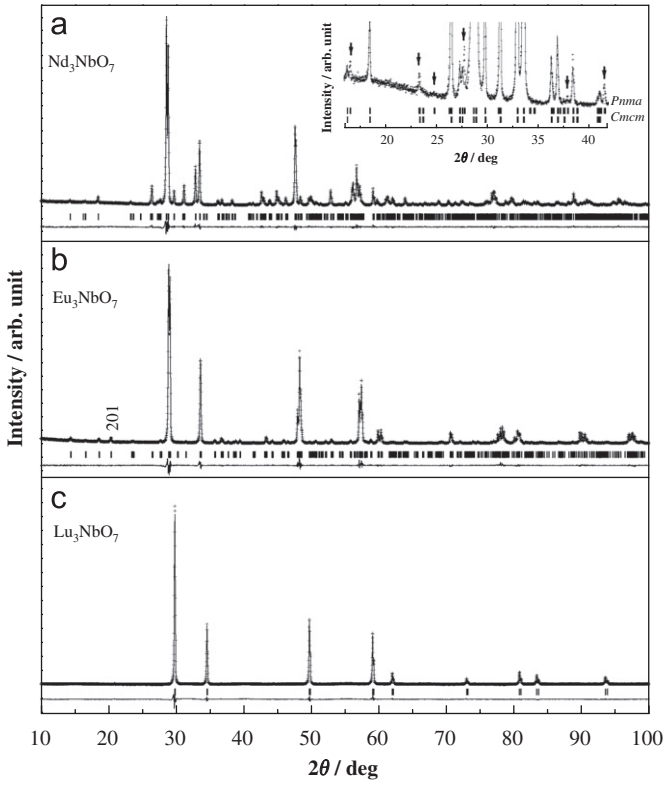

Fig. 1. Powder X-ray diffraction profiles for (a) Nd_3NbO_7 (space group: *Pnma*), (b) Eu_3NbO_7 ($C222_1$), and (c) Lu_3NbO_7 (*Fm*-3*m*; defect-fluorite). The calculated and observed diffraction profiles are shown on the top as a solid line and cross markers, respectively. The vertical markers show positions calculated from Bragg reflections. The bottom trace is a plot of the difference between the calculated and observed intensities. The inset of (a) shows the comparison between two structural models; the solid line on the top represents the calculated profile for the *Cmcm* model. Arrows show the diffraction lines which can be explained by the *Pnma* model (see text).

Table 1
Structural parameters for Nd_3NbO_7.

Atom	Site	*x*	*y*	*z*	B/Å^{2a}
Nd(1)	4*c*	0.0076(3)	1/4	0.7760(1)	0.24(2)
Nd(2)	8*d*	0.2509(2)	0.4771(1)	0.4541(1)	0.24
Nb	4*c*	0.0012(6)	1/4	0.2528(3)	0.16(4)
O(1)	8*d*	−0.050(2)	0.377(1)	0.426(1)	0.9(1)
O(2)	8*d*	−0.030(2)	0.871(1)	−0.062(1)	0.9
O(3)	8*d*	0.241(3)	0.3814(8)	0.724(1)	0.9
O(4)	4*c*	0.261(3)	1/4	0.314(1)	0.9

Note: Space group *Pnma*; $a = 7.6241(1)$ Å, $b = 10.9063(2)$ Å, $c = 7.5247(2)$ Å, $R_{wp} = 8.17\%$, $R_p = 5.96\%$, $R_I = 1.55\%$, $R_e = 6.10\%$.
[a] For the same ions, B values were fixed to be equal.

The crystal structures for Nd_3NbO_7 (*Pnma*) and Eu_3NbO_7 ($C222_1$) are illustrated in Fig. 2. Both structures have similar features: two kinds of infinite chains formed by corner-sharing NbO_6 octahedra and edge-sharing $Ln(1)O_8$ cubes, the slabs consisting of alternate chains, and 7-coordinated $Ln(2)$ ions existing between the slabs. For these two structures, the NbO_6

Table 2
Structural parameters for Eu_3NbO_7.

Atom	Site	x	y	z	B/Å^{2a}
Eu(1)	4*b*	0	0.4954(9)	1/4	0.10(2)
Eu(2)	8*c*	0.2338(1)	0.2349(2)	0.0002(4)	0.10
Nb	4*b*	0	−0.0005(9)	1/4	0.02(6)
O(1)	8*c*	0.129(2)	0.177(3)	0.273(2)	0.3(1)
O(2)	8*c*	0.116(2)	0.794(2)	0.281(2)	0.3
O(3)	4*a*	0.629(1)	0	0	0.3
O(4)	4*a*	0.365(1)	0	0	0.3
O(5)	4*a*	0.057(2)	0	0	0.3

Note: Space group $C222_1$; $a = 10.6480(2)$ Å, $b = 7.5064(1)$ Å, $c = 7.5829(1)$ Å, $R_{wp} = 8.91\%$, $R_p = 6.44\%$, $R_I = 2.56\%$, $R_e = 6.69\%$.
[a] For the same ions, *B* values were fixed to be equal.

Table 3
Structural parameters for Lu_3NbO_7.

Atom	Site	g[a]	x	y	z	B/Å^{2b}
Lu	4*a*	0.75	0	0	0	1.9(1)
Nb	4*a*	0.25	0	0	0	1.9
O	4*b*	0.875	1/4	1/4	1/4	6.5(2)

Note: Space group *Fm*-3*m*; $a = 5.1794(2)$ Å, $R_{wp} = 12.60\%$, $R_p = 8.73\%$, $R_I = 1.76\%$, $R_e = 6.30\%$.
[a] Site occupancy.
[b] For the same ions, *B* values were fixed to be equal.

octahedron and *Ln*(1)O_8 cube in the *Pnma* structure are obviously much more regular than those in the $C222_1$ structure. In the former, the tilting of the NbO_6 chain is along the 0 0 1 direction with the tilting angle (Nb–O–Nb) of 150°–151°, while in the latter, it is along the 1 0 0 direction with the angle of 140°–145°.

Fig. 3 shows the variation of lattice parameters for Ln_3NbO_7 against the ionic radius of the 8-coordinated Ln^{3+} ion [32]. For comparison, all the data are converted to $\sqrt{2}a_f$. The lattice parameters tend to increase with the ionic radius, and the differences among them become larger in order of *Fm*-3*m*, $C222_1$, and *Pnma*. On the border between $C222_1$ and *Pnma* phases, three lattice parameters show the different way of change. The lattice parameters represented by filled squares in Fig. 3 correspond to the axis perpendicular to the slabs consisting of alternate NbO_6 and *Ln*O_8 chains (see Fig. 2) and rapidly increase across the border. In contrast, the other two parameters show only a slight change (open circles: the axis parallel to the chain; open triangles: the axis in the slab and perpendicular to the chain).

The variation of the average interatomic distances against the ionic radii of 8-coordinated Ln^{3+} ion is plotted in Fig. 4. The *Ln*(1)–O, *Ln*(2)–O, and (*Ln*,Nb)–O distances increase with Ln^{3+} ionic radius, while the Nb–O distance is almost constant. For the $C222_1$ and *Pnma* phases, the bond valence sums [33] of *Ln*(1), *Ln*(2), and Nb were calculated to be 2.9–3.1, 2.6–2.8, and 5.0–5.3, respectively. This result is reasonable for the fact that the *Ln* and Nb ions are in the trivalent and pentavalent states, respectively.

3.2. Magnetic properties of Ln_3NbO_7

3.2.1. Paramagnetic behavior

Figs. 5–7 shows the temperature dependence of the magnetic susceptibility (χ_M) or inverse susceptibility (χ_M^{-1}) for Ln_3NbO_7. The effective magnetic moments (μ_{eff}) and Weiss constants (θ) were determined by the Curie–Weiss law using the data between 200 and 400 K. In addition, the Weiss constants at lower temperatures (θ_{LT}) were also obtained from the data in the temperature range

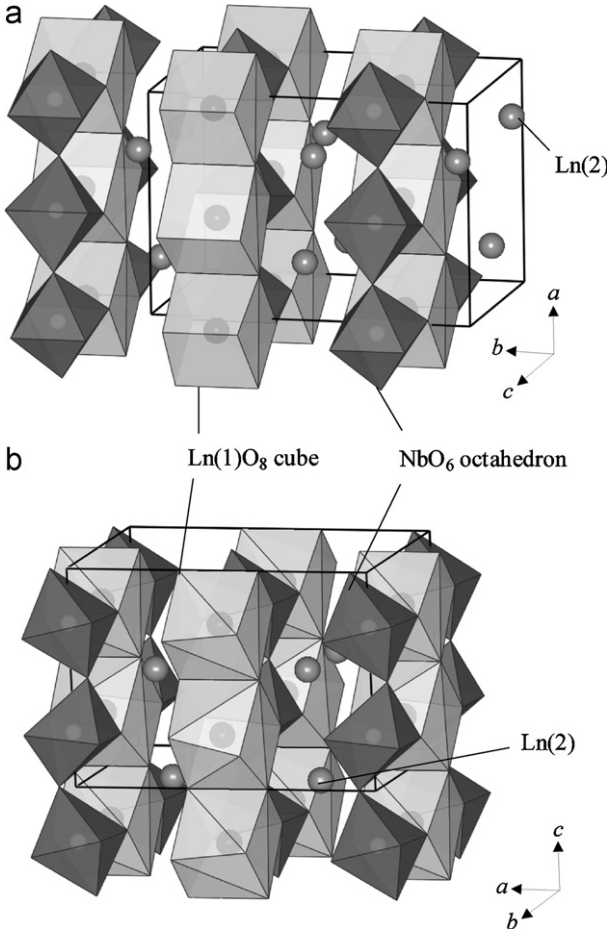

Fig. 2. Schematic crystal structures of (a) Nd_3NbO_7 (*Pnma*) and (b) Eu_3NbO_7 ($C222_1$).

1.8–10 K; they are listed in Table 4. For Sm_3NbO_7 and Eu_3NbO_7, the data do not obey the Curie–Weiss law and show well-known van Vleck paramagnetism due to the behavior of Sm^{3+} and Eu^{3+} ions [34]. Their μ_{eff} values are estimated from the data only at room temperature. For all the Ln_3NbO_7, the μ_{eff} values are very close to calculated moments for free Ln^{3+} ions. The negative Weiss constants indicate that the predominant magnetic interaction between Ln^{3+} ions is antiferromagnetic.

Among Ln_3NbO_7 compounds, the Nd_3NbO_7 and Tb_3NbO_7 show magnetic anomalies in the magnetic susceptibility (see the inset of Fig. 7), and the others are paramagnetic down to 1.8 K. For these two compounds, the specific heat measurements at low temperatures (0.5–25 K) were also carried out.

3.2.2. Magnetic transition in Nd_3NbO_7

The temperature dependence of the magnetic susceptibility and specific heat for Nd_3NbO_7 in the low temperature region is plotted in Figs. 8(a) and (b), respectively. The magnetic susceptibility shows an antiferromagnetic transition at 2.7 K, and below 2.2 K it begins to increase again with decreasing temperature. In the specific heat, a large sharp peak is observed at 2.7 K, and a small broad peak is also observed at 0.6 K. These results indicate that this compound exhibits a two-step antiferromagnetic transition [28].

In order to obtain further information about this behavior, the magnetic entropy (S_{mag}) was calculated from the specific heat data using the equation of $S_{mag} = \int_0^T (C_{mag}/T)\,dT$. The magnetic

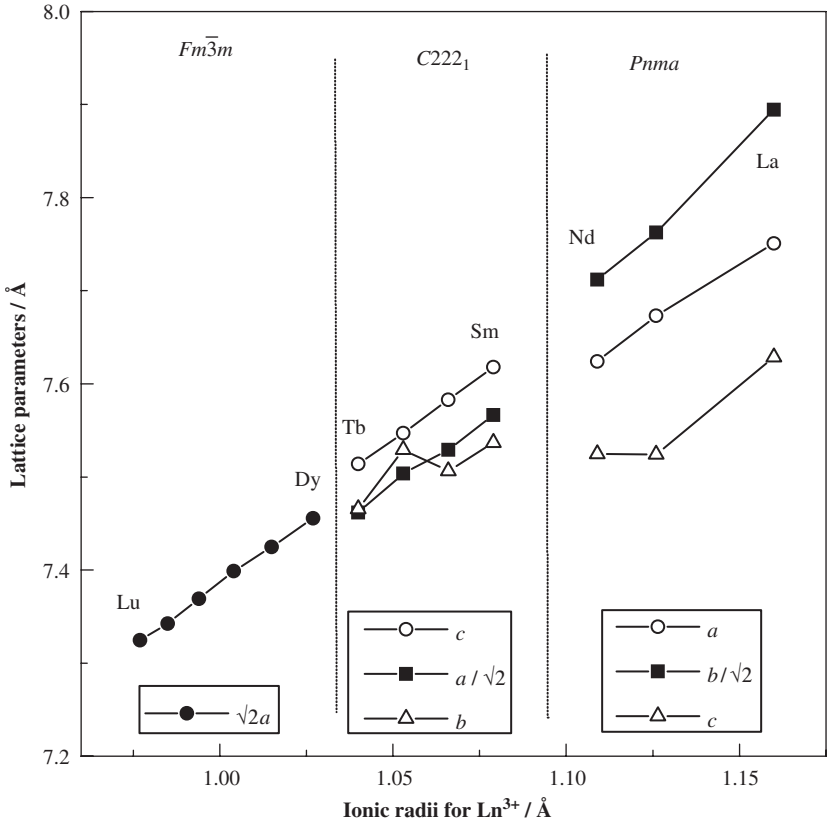

Fig. 3. Variation of lattice parameters for the Ln_3NbO_7 compounds with ionic radii of 8-coordinate Ln^{3+} ions.

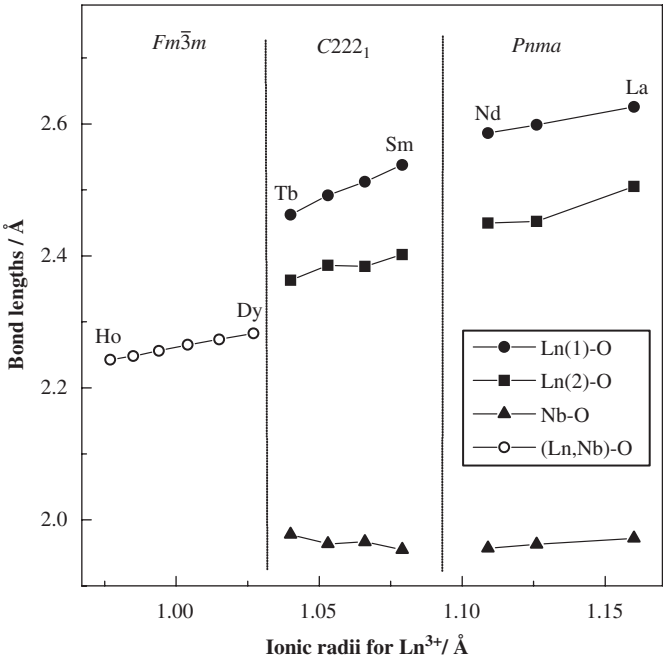

Fig. 4. Variation of the average interatomic distances for the Ln_3NbO_7 compounds with ionic radii of 8-coordinate Ln^{3+} ions.

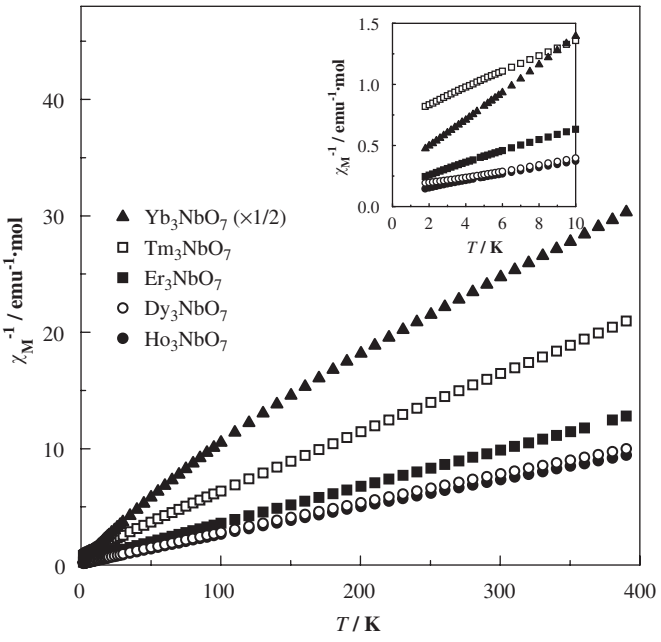

Fig. 5. Temperature dependence of the inverse magnetic susceptibility for Ln_3NbO_7 (Ln = Dy–Yb). The inset shows the detailed inverse magnetic susceptibility below 10 K.

specific heat (C_{mag}) was obtained from $C_{mag} = C_p - C_{lat}$, and for the lattice contribution (C_{lat}) the data of a diamagnetic and isostructural compound La_3NbO_7 was used (see the solid line in the inset graph of Fig. 8(b)). In addition, the magnetic specific heat below 0.5 K was extrapolated by $C_{mag} \propto T^3$ from the spin-wave model for an antiferromagnet [35].

The temperature dependence of the magnetic entropy is shown in Fig. 8(c). The magnetic entropy change (ΔS_{mag})

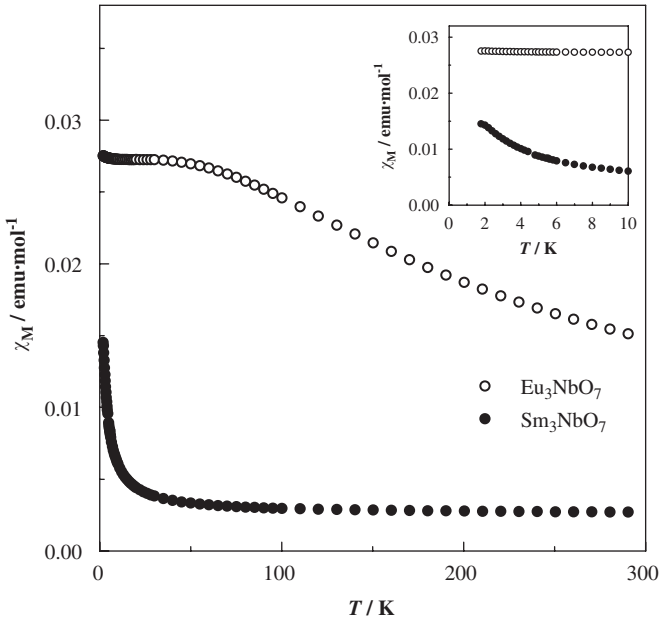

Fig. 6. Temperature dependence of the magnetic susceptibility for Ln_3NbO_7 (Ln = Sm, Eu). The inset shows the detailed magnetic susceptibility below 10 K.

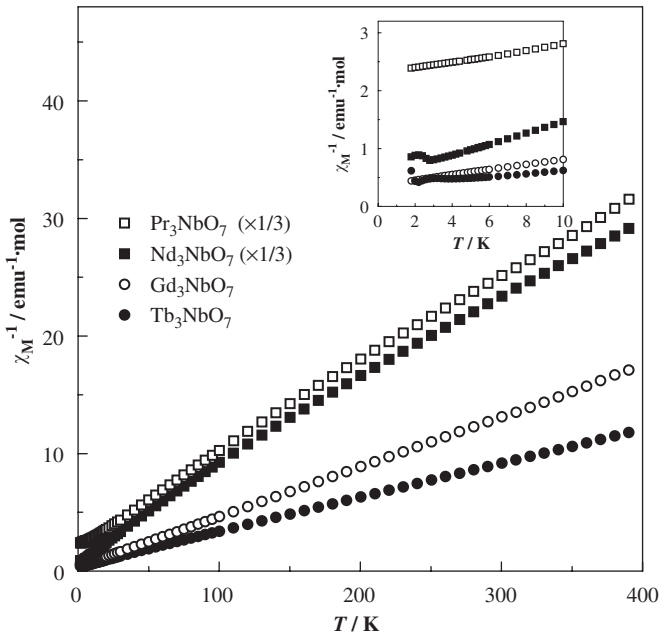

Fig. 7. Temperature dependence of the inverse magnetic susceptibility for Ln_3NbO_7 (Ln = Pr, Nd, Gd, Tb). The inset shows the detailed inverse magnetic susceptibility below 10 K.

associated with the sum of two magnetic anomalies (at 0.6 and 2.7 K) is determined to be 17.0 J mol^{-1} K^{-1}. The Nd^{3+} ions in the Nd_3NbO_7 occupy two crystallographic sites, the 8-coordinated $Ln(1)$ ($4c$) site and 7-coordinated $Ln(2)$ ($8d$) site, with the 1:2 ratio. In both sites, the ground multiplet $^4I_{9/2}$ of the Nd^{3+} ion should split into five Kramers doublets by the crystal field in the orthorhombic symmetry. At sufficiently low temperatures, only the lowest doublet of each Nd^{3+} ions needs to be considered. The observed value of ΔS_{mag} is very close to $3R\ln 2 = 17.3$ J mol^{-1} K^{-1}, which indicates that the ground doublets for three Nd^{3+} ions cause the antiferromagnetic ordering.

Table 4
The effective magnetic moments (μ_{eff}: experimental, μ_{cal}: calculated) per Ln ion, Weiss constant (θ, θ_{LT}), and Néel temperature (T_N) for Ln_3NbO_7.

Compound	μ_{eff}/μ_B	μ_{cal}/μ_B	θ/K	θ_{LT}[c]/K	T_N/K
Pr_3NbO_7	3.59(1)	3.58	−60(1)		
Nd_3NbO_7	3.72(1)	3.62	−58(1)	−5.2(1)	0.6, 2.6
Sm_3NbO_7	1.48[a]	1.55[b]		−4.2(2)	
Eu_3NbO_7	3.45[a]	3.40[b]			
Gd_3NbO_7	7.88(1)	7.94	−5.0(7)	−8.2(1)	
Tb_3NbO_7	9.64(1)	9.72	−19.0(3)	−8.8(1)	2.2, 3.9
Dy_3NbO_7	10.49(1)	10.63	−21.3(9)	−5.7(1)	
Ho_3NbO_7	10.74(1)	10.58	−16.9(5)	−3.85(7)	
Er_3NbO_7	9.19(1)	9.59	−13.0(8)	−3.62(7)	
Tm_3NbO_7	7.32(1)	7.55	−30(1)		
Yb_3NbO_7	4.62(1)	4.54	−92(1)	−2.4(1)	

[a] Observed values at room temperature.
[b] Calculated values by van Vleck [34].
[c] Weiss constants obtained from low temperature data (10–20 K for Nd_3NbO_7 and Tb_3NbO_7 and 1.8–10 K for the others).

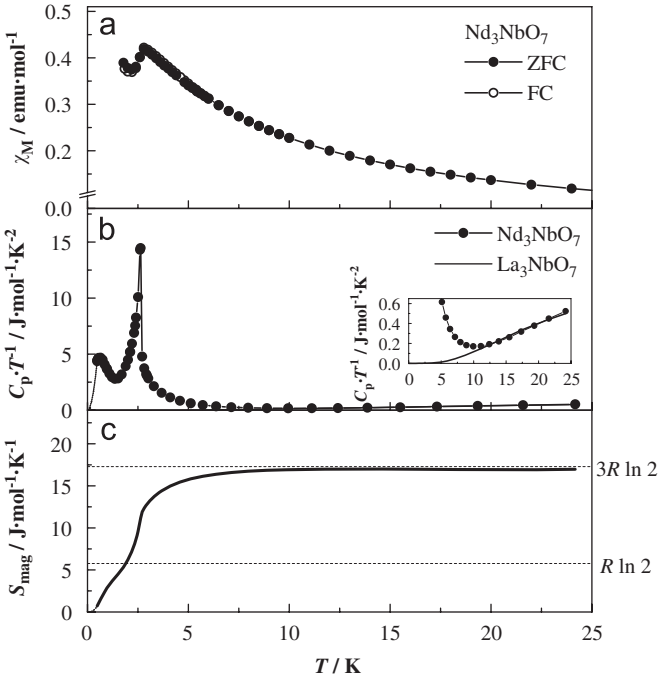

Fig. 8. Temperature dependence of (a) the magnetic susceptibility, (b) specific heat divided by temperature, and (c) magnetic entropy for Nd_3NbO_7. The inset of (b) shows the detailed dependence between 5 and 25 K.

In addition, the magnetic entropy seems to show a step-wise increase ($R\ln 2$+$2R\ln 2$) corresponding to two specific heat anomalies at 0.6 and 2.7 K, respectively. This experimental result suggests that the anomalies observed at 0.6 and 2.7 K are due to the antiferromagnetic ordering of Ln^{3+} ions independently in the 8-coordinated $Ln(1)$ and 7-coordinated $Ln(2)$ sites, respectively. Such a two-step antiferromagnetic transition was also found in the Ta compound Nd_3TaO_7 with a similar crystal structure [28]. Interestingly, the order of occurrence of the transitions is in reverse, i.e., the antiferromagnetic ordering of Nd^{3+} ions at the 8-coordinate site occur at 2.6 K and the 7-coordinated Nd^{3+} ions order at 2.1 K in the Nd_3NbO_7 compound. At present, it is difficult to explain the reason for this difference. Small difference in the crystal structure (*Pnma* for Nd_3NbO_7 and *Cmcm* for Nd_3TaO_7) may strongly affect the magnetic interaction between Nd ions.

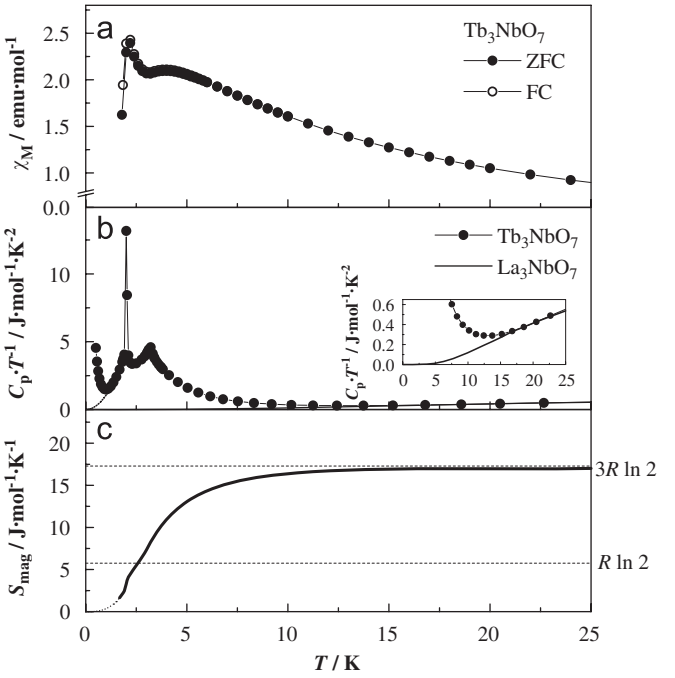

Fig. 9. Temperature dependence of (a) the magnetic susceptibility, (b) specific heat divided by temperature, and (c) magnetic entropy for Tb_3NbO_7. The inset of (b) shows the detailed dependence between 5 and 25 K.

3.2.3. *Magnetic transition in Tb_3NbO_7*

Fig. 9(a) shows the temperature dependence of the magnetic susceptibility for the Tb_3NbO_7 below 25 K. The magnetic susceptibility shows a broad maximum around 4 K and a cusp at 2 K. In the specific heat data (Fig. 9(b)), corresponding anomalies are observed as peaks at 3.2 and 2.0 K, respectively. These anomalies indicate that the two-step antiferromagnetic transition also occurs in this compound. The Ta analog Tb_3TaO_7, which has the same crystal structure (space group $C222_1$), also shows a similar specific heat behavior [28].

Below ~1 K, the specific heat turns to increase with decreasing temperature. This increasing can be ascribed to the Zeeman splitting of ^{159}Tb nuclei (abundance ratio: 100%) with $I = 3/2$, which is derived from the internal magnetic field by the magnetic ordering of Tb^{3+} ions. To eliminate this contribution, the data was extrapolated by assuming $C_{mag} \propto T^3$ (the dotted curve in Fig. 9(b)) [35].

The temperature dependence of the magnetic entropy for the Tb_3NbO_7 was calculated by the same way as the case for the Nd_3NbO_7, and it is plotted as a solid line in Fig. 9(c). The total ΔS_{mag} is determined to be 17.0 J mol^{-1} K^{-1} per formula unit, which is good agreement with 17.4 J mol^{-1} K^{-1} (at 15 K) found in the Ta analog. The Tb^{3+} ion is a non-Kramers ion, and its ground multiplet $^7F_6$ should split into many states by the crystal field. Among the combinations (for Tb(1) and Tb(2) sites) of the possible degeneracy of the Tb^{3+} ion ($W = 1$–6), only $R\ln 2 + 2R\ln 2 = 17.3$ J mol^{-1} K^{-1} ($W_1 = W_2 = 2$) is reasonable for the obtained ΔS_{mag} value. Therefore, it is considered that non-Kramers doublets of Tb^{3+} ions at each site individually cause the antiferromagnetic ordering.

In the specific heat data (Fig. 9(b)), the peak observed at 2.0 K is extremely sharp, while the peak at 3.2 K is somewhat broad. The latter spreads up to ~15 K, which may indicate that the onset of short-range magnetic ordering occurs around this temperature. Owing to the difficulty in dividing the magnetic entropy data into these two anomalies, we cannot determine the individual ΔS_{mag} values. At least, we can say that ΔS_{mag} due to the magnetic anomaly at 2.0 K seems to be much smaller than that at 3.2 K, which indicates that the antiferromagnetic ordering of the Tb^{3+} ions occupying the *Ln*(1) and *Ln*(2) sites occurs at 2.0 and 3.2 K, respectively. This result is almost the same as the Tb_3TaO_7 (*Ln*(1): 2.9 K, *Ln*(2): 3.6 K) [28]. With decreasing temperature, the 7-coordinated *Ln* ions show the magnetic transition first and then the 8-coodinated *Ln* ions order antiferromagnetically.

4. Summary

The XRD measurements and Rietveld analyzes show that ternary compounds Ln_3NbO_7 adopt the fluorite-related structures with the space group *Pnma* (*Ln* = La, Pr, Nd), $C222_1$ (*Ln* = Sm–Tb), or *Fm*-3*m* (*Ln* = Dy–Lu). The Ln_3NbO_7 for *Ln* = Pr, Sm–Gd, Dy–Yb are paramagnetic down to 1.8 K, while the Nd and Tb compounds show antiferromagnetic behavior at very low temperatures. From the specific heat measurements, it is found that the latter two compounds show "two-step" antiferromagnetic transitions due to the long-range antiferromagnetic ordering of *Ln* ions in different crystallographic sites.

Acknowledgments

This research was partially supported by Grant-in-aid for Scientific Research (no. 20550052) and Global COE Program (Project no. B01: Catalysis as the Basis for Innovation in Materials Science) from the Ministry of Education, Culture, Sports, Science and Technology of Japan.

Appendix A. Supplementary material

Supplementary data associated with this article can be found in the online version at doi:10.1016/j.jssc.2008.12.012.

References

[1] H.P. Rooksby, E.A.D. White, J. Am. Ceram. Soc. 47 (1964) 94–96.
[2] G. Garton, B.M. Wanklyn, J. Mater. Sci. 3 (1968) 395–401.
[3] G. Tilloca, M. Perez, Y. Jorba, F. Queyroux, CR. Acad. Sci. C 271 (1970) 134–135.
[4] J.G. Allpress, H.J. Rossell, J. Solid State Chem. 27 (1979) 105–114.
[5] H.J. Rossell, J. Solid State Chem. 27 (1979) 115–122.
[6] A.N. Klimenko, Y. Kozlov, V.S. Sergeev, E.A. Pastukhov, Thermochim. Acta 209 (1992) 331–338.
[7] J.F. Vente, R.B. Helmholdt, D.J.W. Ijdo, J. Solid State Chem. 108 (1994) 18–23.
[8] A. Kahn-Harari, L. Mazerolles, D. Michel, F. Robert, J. Solid State Chem. 116 (1995) 103–106.
[9] L. Cai, C. Nino, J. Eur. Ceram. Soc. 27 (2007) 3971–3976.
[10] J.E. Greedan, N.P. Raju, A. Wegner, P. Gougeon, J. Padiou, J. Solid State Chem. 129 (1997) 320–327.
[11] H. Nishimine, M. Wakeshima, Y. Hinatsu, J. Solid State Chem. 178 (2005) 1221–1229.
[12] F.P.F. van Berkel, D.J.W. IJdo, Mater. Res. Bull. 21 (1986) 1103–1106.
[13] P. Khalifah, R.W. Erwin, J.W. Lynn, Q. Huang, B. Batlogg, R.J. Cava, Phys. Rev. B 60 (1999) 9573.
[14] P. Khalifah, Q. Huang, J.W. Lynn, R.W. Erwin, R.J. Cava, Mater. Res. Bull. 35 (2000) 1–7.
[15] R.P. Bontchev, A.J. Jacobson, M.M. Gospodinov, V. Skumryev, V.N. Popov, B. Lorenz, R.L. Meng, A.P. Litvinchuk, M.N. Iliev, Phys. Rev. B 62 (2000) 12235.
[16] D. Harada, Y. Hinatsu, J. Solid State Chem. 158 (2001) 245–253.
[17] D. Harada, Y. Hinatsu, Y. Ishii, J. Phys. Condens. Matter 13 (2001) 10825–10836.
[18] D. Harada, Y. Hinatsu, J. Solid State Chem. 164 (2002) 163–168.
[19] R. Lam, F. Wiss, J.E. Greedan, J. Solid State Chem. 167 (2002) 182–187.
[20] J.F. Vente, D.J.W. IJdo, Mater. Res. Bull. 26 (1991) 1255–1262.
[21] H. Nishimine, M. Wakeshima, Y. Hinatsu, J. Solid State Chem. 177 (2004) 739–744.
[22] H. Nishimine, Y. Doi, Y. Hinatsu, M. Sato, J. Ceram. Soc. Jpn. 115 (2007) 577–581.
[23] J.R. Plaisier, R.J. Drost, D.J.W. Ijdo, J. Solid State Chem. 169 (2002) 189–198.

[24] W.R. Gemmill, M.D. Smith, Y.A. Mozharivsky, G.J. Miller, H.C. zur Loye, Inorg. Chem. 44 (2005) 7047–7055.
[25] R. Lam, T. Langet, J.E. Greedan, J. Solid State Chem. 171 (2003) 317–323.
[26] Y. Hinatsu, M. Wakeshima, N. Kawabuchi, N. Taira, J. Alloys Compd. 374 (2004) 79–83.
[27] M. Wakeshima, Y. Hinatsu, J. Solid State Chem. 179 (2006) 3575–3581.
[28] M. Wakeshima, H. Nishimine, Y. Hinatsu, J. Phys. Condens. Matter 16 (2004) 4103–4120.
[29] J.D. Cashion, A.H. Cooke, M.J.M. Leask, T.L. Thorp, M.R. Wells, J. Mater. Sci. 3 (1968) 402–407.
[30] A.I. Komkov, Doklady Akademii Nauk 126 (1959) 853–854.
[31] F. Izumi, T. Ikeda, Mater. Sci. Forum 321–324 (2000) 198–203.
[32] R.D. Shannon, Acta. Crystallogr. A 32 (1976) 751–767.
[33] I.D. Brown, A. Altermatt, Acta Crystallogr. B 41 (1985) 244–247.
[34] J.H. van Vleck, The Theory of Electric and Magnetic Susceptibilities, Clarendon, Oxford, 1932.
[35] S.J. Joshua, A.P. Cracknell, Phys. Lett. A 28 (1969) 562–563.